Received: 14 September 2020 | Revised: 17 February 2021 | Accepted: 27 February 2021

DOI: 10.1002/hbm.25406

RESEARCH ARTICLE

WILEY

Early-stage Parkinson's disease: Abnormal nigrosome 1 and 2 revealed by a voxelwise analysis of neuromelanin-sensitive MRI

Young Hee Sung[1] | Young Noh[1] | Eung Yeop Kim[2]

[1]Department of Neurology, Gil Medical Center, Gachon University College of Medicine, Incheon, Republic of Korea

[2]Department of Radiology, Samsung Medical Center, Sungkyunkwan University School of Medicine, Samsung Medical Center, Gangnam-gu, Seoul, Republic of Korea

Correspondence
Eung Yeop Kim, Department of Radiology, Samsung Medical Center, Sungkyunkwan University School of Medicine, 81 Irwon-ro, Gangnam-gu, Seoul 06351, Republic of Korea.
Email: neuroradkim@gmail.com

Funding information
The Brain Research Program of the National Research Foundation, Grant/Award Number: 2018M3C7A1056889; The Korea Healthcare Technology R&D Project, Grant/Award Number: HI14C1135

Abstract

Previous pathologic studies evaluated the substantia nigra pars compacta (SNpc) of a limited number of idiopathic Parkinson's disease (IPD) patients with relatively longer disease durations. Therefore, it remains unknown which region of the SNpc is most significantly affected in early-stage IPD. We hypothesized that a voxelwise analysis of thin-section neuromelanin-sensitive MRI (NM-MRI) may help determine the significantly affected regions of the SNpc in early-stage IPD and localize these areas in each nigrosome on high-spatial-resolution susceptibility map-weighted imaging (SMwI). Ninety-six healthy subjects and 50 early-stage IPD patients underwent both a $0.8 \times 0.8 \times 0.8$ mm^3 NM-MRI and a $0.5 \times 0.5 \times 1.0$ mm^3 multi-echo gradient-recalled echo imaging for SMwI. Both NM-MRI and SMwI templates were created by using image data from the 96 healthy subjects. Permutation-based nonparametric tests were conducted to investigate spatial differences between the two groups in NM-MRI, and the results were displayed on both NM-MRI and SMwI templates. The posterolateral and anteromedial regions of the SNpc in NM-MRI were significantly different between the two groups, corresponding to the nigrosome 1 and nigrosome 2 regions, respectively, on the SMwI template. There were the areas of significant spatial difference in the hypointense SN on SMwI between early-stage IPD patients and healthy subjects. These areas on SMwI were slightly greater than those on NM-MRI, including the areas showing group difference on NM-MRI. Our voxelwise analysis of NM-MRI suggests that two regions (nigrosome 1 and nigrosome 2) of the SNpc are separately affected in early-stage IPD.

KEYWORDS
magnetic resonance imaging, neuromelanin, nigrosome, Parkinson disease, substantia nigra pars compacta

1 | INTRODUCTION

In a previous study, it was shown that loss of pigmented neurons in the substantia nigra pars compacta (SNpc) in idiopathic Parkinson's disease (IPD) is greatest in the lateral ventral tier, followed by the medial ventral tier and the dorsal tier (Fearnley & Lees, 1991). This study had the involvement of 20 patients who had had IPD for 15 ± 10 years, but it did not show if there is regional selectivity in

This is an open access article under the terms of the Creative Commons Attribution-NonCommercial-NoDerivs License, which permits use and distribution in any medium, provided the original work is properly cited, the use is non-commercial and no modifications or adaptations are made.
© 2021 The Authors. *Human Brain Mapping* published by Wiley Periodicals LLC.

early-stage IPD. Another pathological study suggested that cell loss progressively occurs in the order of nigrosome 1, 2, 4, 3, and 5 (Damier, Hirsch, Agid, & Graybiel, 1999). This study with five patients with IPD was limited because the duration of them was 7 to 32 years. In fact, it is extremely difficult to assess fresh brain tissues from patients with early-stage IPD because of rare autopsies on them. Thus, it would be better to find an alternative method to elucidate which subregion of the SNpc is most affected in early-stage IPD.

Given that a recent study showed that the signal intensity in neuromelanin-sensitive MRI (NM-MRI) is correlated with NM concentration (Cassidy et al., 2019), an analysis using NM-MRI may help determine which area is most impacted in early-stage IPD. In previous studies, in order to determine abnormality in the SNpc, a contrast ratio (CR) was measured in the two or three subdivisions of the SNpc (Fabbri et al., 2017; Ohtsuka et al., 2014; Prasad et al., 2018; Wang et al., 2018; Xiang et al., 2017), or a whole or regional volume of the SN was calculated using a specific threshold (Castellanos et al., 2015; Isaias et al., 2016; Kashihara, Shinya, & Higaki, 2011; Kuya et al., 2018; Le Berre et al., 2019; Matsusue et al., 2019; Ogisu et al., 2013; Okuzumi et al., 2019; Pyatigorskaya et al., 2018; Reimao, Pita Lobo, Neutel, Correia Guedes, et al., 2015; Reimao, Pita Lobo, Neutel, Guedes, et al., 2015; Schwarz et al., 2011; Schwarz, Xing, Tomar, Bajaj, & Auer, 2017; Takahashi et al., 2018; Taniguchi et al., 2018; Vitali et al., 2020; Zupan, Suput, Pirtosek, & Vovk, 2019), and the values were compared between IPD patients and healthy subjects. These results failed to specify the most affected region of the SNpc. Although previous studies have shown the potential of NM-MRI as a diagnostic imaging biomarker, they have some methodological concerns; for example, the measurements of CRs or volumes of the SNpc in NM-MRI were not based on a voxelwise analysis using a template, which may lead to measurement errors. Additionally, given the size and shape of the SNpc, it is prone to being affected by the partial-volume effect, which results in lower reliability. In fact, a recent study recommended 1.5 mm thick NM-MRI for voxelwise analysis of the SNpc (Wengler, He, Abi-Dargham, & Horga, 2020). Most of the previous studies, however, obtained relatively thick-slice (2–3 mm) imaging. Despite two studies based on a voxelwise analysis being conducted recently, they showed discrepant results. One of them suggested that the anterolateral aspect of the SNpc, not fully involving the posterior SNpc, is the most affected region in a relatively small number of patients with longer disease duration (n = 28, mean of 7.3 years; Cassidy et al., 2019); whereas the other study claimed that the posterolateral areas of the SNpc are the primary sites in early-stage IPD (Biondetti et al., 2020). These studies involved use of a 3 mm NM-MRI and had IPD patients with different disease durations. The posterior aspect of the SNpc includes an area of hyperintensity on susceptibility-weighted imaging (SWI), which is known to be lost in IPD (Mahlknecht, Krismer, Poewe, & Seppi, 2017). As in NM-MRI studies, the results obtained through SWI have not been confirmed by pathological analyses or a voxelwise analysis using NM-MRI. Determining the precise location of the affected regions of the SNpc in early-stage IPD may have clinical implications, because they can serve as a region of interest to measure CRs for both diagnosis and longitudinal study. Thus, the aim of our study was to conduct a voxelwise analysis using 0.8 mm isovoxel NM-MRI on early-stage IPD patients, in order to find the most significantly affected region in the SNpc.

2 | METHODS

2.1 | Participants

We retrospectively enrolled 50 consecutive patients, who visited our movement disorder clinic and were diagnosed as IPD in the period between January 2018 and October 2019. All patients underwent both head MRI and N-3-fluoropropyl-2-b-carbomethoxy-3-b-(4-iodophenyl) nortropane PET (18F-FP-CIT PET) for the initial diagnosis. Patients with normal 18F-FP-CIT PET were excluded, in accordance with the Movement Disorder Society clinical diagnostic criteria for Parkinson's disease (Postuma et al., 2015). Motor symptoms were assessed using the Hoehn and Yahr scales (Hoehn & Yahr, 1967) and Unified Parkinson's Disease Rating Scale (UPDRS). All 50 IPD patients were drug-naïve. The clinical laterality of motor symptoms was evaluated by using the scores of UPDRS III. Scores of resting tremor, rigidity, finger tapping, hand movement, and rapid alternative movements of hand and leg agility were summed in the right and left sides separately. When the score of one side was higher than that of the other side by two points, the higher score side decided as dominant side. The association between handedness and clinical laterality of IPD patients was assessed by using the Fisher's Exact test. We also enrolled 96 healthy subjects to create unbiased NM-MRI and susceptibility map-weighted MRI (SMwI) templates. Healthy subjects were participants of the Environmental Pollution-Induced Neurological EFfects (EPINEF) study, which is based on community. Through local advertisements, individuals without known neurological diseases (e.g., any kind of dementia, movement disorders, or stroke) were recruited and enrolled in this cohort (Cho et al., 2020). The 96 participants in the healthy group did not have subjective memory complaints and objective cognitive decline. All of them had a Clinical Dementia Rating (CDR) score of 0 and normal results on neuropsychological tests (defined as within 1.5 *SDs* of age- and education-corrected normative mean). Participants were excluded if they had structural abnormalities in MRI such as intracranial hemorrhage, cerebral, cerebellar, or brainstem infarction, traumatic brain injury, hydrocephalus, tumors, severe white matter hyperintensity, white matter hyperintensity associated with radiation, multiple sclerosis, or vasculitis. Fifty healthy age- and sex-matched subjects were selected to compare with the 50 patients with early-stage IPD (Table 1).

2.2 | Imaging acquisition

All participants underwent MR imaging at a 3 T scanner with a 32-channel coil (Skyra; Siemens Healthineers, Forchheim, Germany). All participants gave informed consent.

TABLE 1 Demographics and clinical characteristics of the study population

	IPD (n = 50)	Healthy subjects (n = 50)	p value
Age (years)	69.0 (58.3–78.0)	67 (63.3–71.8)	.320
Sex (male: Female)	23:27	16:34	.373
Disease duration (months)	6 (3.3–12.0)	–	–
Hoehn and Yahr stage	2 (1–2)	–	–
UPDRS I	0 (0–2)	–	–
UPDRS II	6 (4–7)	–	–
UPDRS IIII	13 (9–21)	–	–
Handedness (right: Left)	45:5	47:3	1.00
Clinical laterality	Right, 31 Left, 11 No laterality, 8	–	–

Note: Data are median, with interquartile ranges in parentheses.
Abbreviations: IPD, idiopathic Parkinson's disease; UPDRS, unified Parkinson's disease rating scale.

Whole-brain sagittal 3D magnetization prepared rapid gradient echo (MP-RAGE) imaging was first obtained with the following parameters: repetition time (TR), 1800 ms; echo time (TE), 3 ms; inversion time (TI), 920 ms; matrix 256 × 256; field of view (FOV), 250 × 250; acceleration factor of two; and acquisition time, 3 min and 35 s.

Oblique axial three-dimensional multi-echo gradient-recalled echo (GRE) imaging was obtained parallel to the plane from the posterior commissure and top of the pons, which was localized using the sagittal MP-RAGE (see Figure S1). The parameters of the 3D multi-echo GRE imaging were as follows: TR, 48 ms; minimum TE, 14.38 ms; echo train length, 3; echo spacing, 12.3 ms; matrix 384 × 384; FOV, 192 × 192 (100% phase resolution); slice thickness, 1 mm; slice number, 32; acceleration factor of two; and acquisition time, 4 min and 46 s.

Both magnitude and phase images of multi-echo GRE imaging were used to reconstruct quantitative susceptibility mapping (QSM). The iterative least-square method was used to reconstruct QSM for all image data. SMwI images were reconstructed using QSM as a mask. This approach further enhances susceptibility contrast and helps to better visualize the nigrosome regions. More details for reconstructing SMwI can be found in other studies (Gho et al., 2014; Nam, Gho, Kim, Kim, & Lee, 2017).

Three-dimensional T1-weighted sampling perfection with application optimized contrast using different flip-angle evolutions (SPACE) imaging was obtained at the same imaging plane for multi-echo GRE, with the following parameters: TR, 900 ms; TE, 4.8 ms; echo spacing, 4.76 ms; echo train duration, 338 ms; variable flip angle; delay alternating with nutation for tailored excitation (DANTE) preparation to improve delineation of the substantia nigra pars compacta (Oshima et al., 2020); matrix 288 × 288; field of view (FOV), 230 × 230 (100% slice/phase resolution); slice thickness, 0.8 mm; slice number, 208; acceleration factor of two (Controlled Aliasing in Parallel Imaging Results in Higher Acceleration—CAIPIRINHA); and acquisition time, 5 min and 12 s (see representative images in Figure S2). We chose to use T1-weighted SPACE with DANTE preparation in this study because we were able to obtain faster high-spatial-resolution imaging, which has shown a comparable diagnostic performance to gradient-recalled echo imaging with magnetization transfer (Oshima et al., 2020).

All patients with IPD also underwent N-3-fluoropropyl-2-b-carbomethoxy-3-b-(4-iodophenyl) nortropane PET (18F-FP-CIT PET) at a PET/CT scanner (Biograph-6; Siemens, Erlangen, Germany). Data were collected in the 3D scanning mode with 40 slices (thickness, 3 mm) examined.

2.3 | Preprocessing for creating NM-MRI and SMwI templates

SMwI provides the anatomical information on nigrosomes, but NM-MRI does not. It is therefore necessary to create both NM-MRI and SMwI templates to determine which nigrosome region is most significantly affected on NM-MRI. In this study, the NM-MRI template was used to determine the significantly affected regions of the SNpc in early-stage IPD. The high-spatial-resolution SMwI template was utilized to localize these areas in each nigrosome. The MNI template has been widely used for voxel-based analysis. This template, however, is not suitable for depicting the SNpc because it is made by averaging 3D T1-weighted gradient-recalled echo MRI (e.g., MP RAGE). Intensity-based registration algorithm minimizes the cost function between the source and target images, which in turn leads to poor alignment of the SNpc and affects the accuracy of voxel-based approach. Instead of using a T1-weighted imaging-based template, we simply modified previous methods by changing the normalization target. This specific method can minimize potential errors that can occur in the process of spatial normalization between two different image datasets (i.e., enhances accuracy of co-registration), thereby improving sensitivity for quantification or voxel-based analysis.

Nonuniformity artifacts of all MRIs were first corrected by using the nonparametric nonuniform intensity normalization (N3) algorithm (Sled, Zijdenbos, & Evans, 1998). Thereafter, non-brain tissues were removed by using the BET algorithm (Smith, 2002). The skull-stripped images were registered linearly to a common coordinate space by using version 2.1.52–0 of the Advanced Normalization Tools (ANTs; https://www.nitrc.org/projects/ants), which gave a linear transform matrix. Both NM-MRI

and SMwI were rigidly co-registered to their corresponding individual MRI. The matrices obtained from the above two registration processes were concatenated and applied to both native NM-MRI and SMwI. The area around the brainstem was cropped to reduce the computation burden. A cropping 3D window was selected by a neuroradiologist to include the brainstem area in the Montreal Neurological Institute (MNI) space.

2.4 | Template creation

Twenty sets of the pre-processed images were selected and were registered to a common coordinate space. For signal intensity normalization, mean signal intensity of the registered images was obtained first, which was done by the function, "AverageImages", of the ANTs toolkit. After normalizing their signal intensity, they were averaged to create the initial target template.

We used a symmetric group-wise normalization approach, provided by the ANTs toolkit, to generate unbiased templates for both shape and appearance. The images were processed as follows:

1. Pairwise normalize all 96 preprocessed images with the initial target template.
2. Average the normalized images to create a new target template.
3. Transform the new target template by using both the average affine transformation matrix and the average inverse warp field.
4. Iterate steps 1 to 3.

We repeated the above process 20 times, in which we attempted a hierarchical registration framework. This recovered the largest smooth deformation first, and then finer, more local deformations were finally recovered. The step size used, blurring, and iterations are shown in the Table S1. During the above iterations, both the transformation matrix and warp field applied to the MRI were applied to the corresponding NM-MRI and SMwI. Finally, in order to build a symmetric template, we adopted the method of Fonov et al (Fonov et al., 2011). The two templates created were in the same spatial coordinates with the same shape. The hyperintense areas on the NM-MRI template were superimposed on the SMwI template to see how much they overlapped (in the nigral hyperintensity on the SMwI template in particular), because it has been suggested that there is a substantial discrepancy in the location between the volumes estimated on SWI and NM-MRI (overlap of approximately 12%; Langley et al., 2015).

Voxelwise analysis using contrast ratio (CR) of NM-MRI and SMwI between IPD patients and healthy subjects.

To calculate contrast ratio (CR), all NM-MRI images were spatially normalized with the newly generated NM-MRI template. We placed two background regions of interest (each a 3.5 mm sphere) on both sides of the cerebral peduncle areas on the NM-MRI template (Figure S3). The NM-MRI CR for each voxel (V) was calculated as the relative change in NM-MRI signal intensity (SI) from background region (BG).

$$CR_V = \frac{(SI_V - SI_{BG})}{SI_{BG}}$$

For voxelwise analysis, all NM-MRI data from patients with IPD were spatially normalized to the 0.5 mm isovoxel resampled NM-MRI template with a skull mask. Images were then spatially smoothed with a 1.5 mm full-width-at-half-maximum Gaussian kernel. Finally, an inclusive mask of SN was created by manual tracing on the NM-MRI template. The Randomize tool in FSL was used to conduct permutation-based non-parametric tests (10,000 permutations), in order to investigate spatial differences between healthy subjects and IPD patients. The threshold-free cluster enhancement (TFCE) in FSL was used to find clusters in the data ($p < .05$, TFCE corrected). All SMwI data from patients with IPD were similarly postprocessed. Spatial differences between healthy subjects and IPD patients were also similarly assessed.

Abnormal areas determined from the voxelwise analysis by using the NM-MRI template were superimposed on the SMwI template from healthy subjects. The results were presented at three different imaging planes, including the plane parallel to the anterior commissure-posterior commissure (AC-PC) line, and the planes perpendicular and parallel to the midbrain axis. Using an SMwI template and the anatomical information on nigrosomes 1–5 (Massey et al., 2017), we tried to determine where the abnormal regions were located. Abnormal areas determined from the voxelwise analysis by using the SMwI template were superimposed on the SMwI template from healthy subjects.

The CR values of significant group difference on NM-MRI were assessed if they were correlated with the UPDRS III scores or disease duration.

3 | RESULTS

Of patients with IPD, 45 and five participants were right and left handed, respectively. The right and left dominant clinical laterality was noted in 31 and 11 participants, respectively. Eight patients had no clinical laterality (Table 1). For 42 patients with clinical laterality, there was no significant association between handedness and clinical laterality ($p > .05$, Fisher's Exact test).

The SMwI template overlaid with the NM-MRI template showed that the hyperintense areas on the NM-MRI were partially overlapped with the posteromedial aspect of the hypointense areas on the SMwI, above the lower pole of the red nucleus. The overlap was smaller below the lower pole of the red nucleus, where the hyperintense areas on the NM-MRI template were located in the nigral hyperintensity between the two hypointense layers (Figure 1).

We found that two different regions in each SNpc on NM-MRI were significantly different between early-stage IPD patients and healthy subjects (Figure 2). The ranges of CR values are given in Table 2. The larger abnormal regions were located in the posterolateral aspect of each SNpc, with the region on the left being slightly greater than the one on the right. These abnormal regions in the

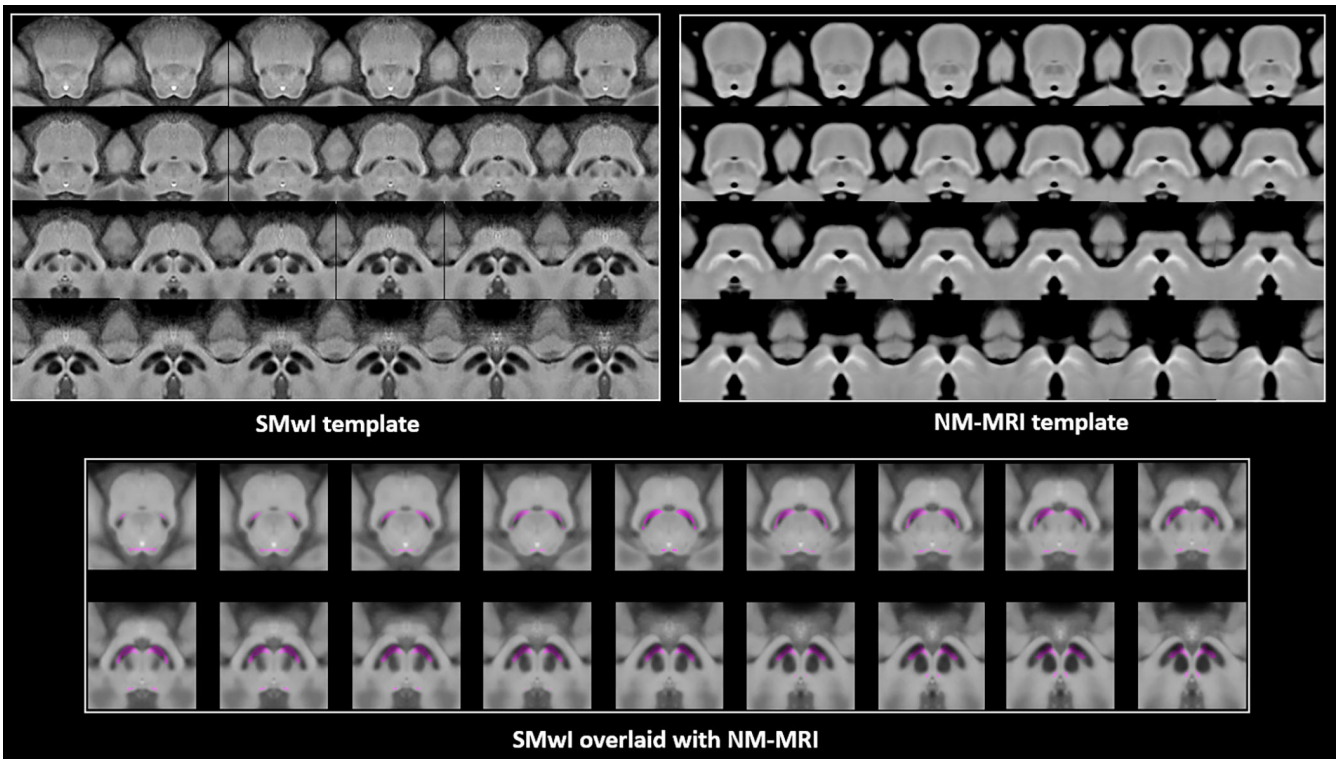

FIGURE 1 SMwI (susceptibility map-weighted imaging) and NM-MRI (neuromelanin-sensitive imaging) templates derived from healthy subjects. All images are displayed using the radiological convention. The SMwI template overlaid with the NM-MRI template shows that the hyperintense areas in the NM-MRI are partially overlapped by the posteromedial aspect of the hypointense areas in SMwI above the lower pole of the red nucleus (the areas in pink are those from the hyperintense substantia nigra on the NM-MRI template). The overlap is smaller below the lower pole of the red nucleus, where the hyperintense areas on the NM-MRI template are located in the nigral hyperintensity between the two hypointense layers

posterior SNpc were noted within the posterior nigral hyperintensity (Figure 3), which has been described as the presumed nigrosome 1 in the previous studies (Massey et al., 2017; Schwarz et al., 2018), The smaller abnormal regions were identified in the anteromedial aspect of the SNpc on both sides (Figure 2). These areas were presumably located in the nigrosome 2 region (Figure 3; Massey et al., 2017; Schwarz et al., 2018). On the plane perpendicular to the midbrain axis, the larger abnormal areas in the SNpc were predominately located inferior to the lower pole of the red nucleus on the SMwI template (Figure S4). For those who are familiar with images obtained parallel to the AC-PC line, the resampled images overlaid with significant spatial differences between IPD and healthy subjects are presented (Figure S5). A box-and-whisker plot of the extracted NM-MRI CR values for each cluster is given (Figure S6). Table 3 shows cluster sizes and *p* values of the significantly different regions on NM-MRI between patients with idiopathic Parkinson's disease and healthy subjects.

There were the areas of significant spatial difference in the hypointense SN on SMwI between early-stage IPD patients and healthy subjects (Figure 4). These areas on SMwI were slightly greater than those on NM-MRI, including the areas showing group difference on NM-MRI. Also seen was that the area on the left is larger than that on the right, which was similarly noted on NM-MRI. The areas showing group difference on SMwI (Figure 4) were slightly larger than the presumed nigrosome 1 and nigrosome 2 regions (Figure 3).

The UPDRS III scores or disease duration were not significantly correlated with the CR values of group difference or the whole SNpc on NM-MRI ($p > .05$).

4 | DISCUSSION

This voxelwise study shows that the significantly affected regions in patients with early-stage IPD are located in the posterolateral aspect of the SNpc on the NM-MRI template, and correspond to the posterior nigral hyperintensity areas on the SMwI template. This significantly affected region is in the posterior aspect of the putative nigrosome 1 area in previous studies (Massey et al., 2017; Schwarz et al., 2018), which is the so-called dorsal nigral hyperintensity (Figure S5; Mahlknecht et al., 2017). Also of note is that the main abnormality was found below the inferior pole of the red nucleus, which supports the previous results (Sung et al., 2018). It should therefore be mentioned that loss of dorsal nigral hyperintensity on SWI should be assessed below the inferior border of the red nucleus.

Additionally, it is worth noting that another small region is significantly impacted in the anteromedial aspect of the SNpc in patients

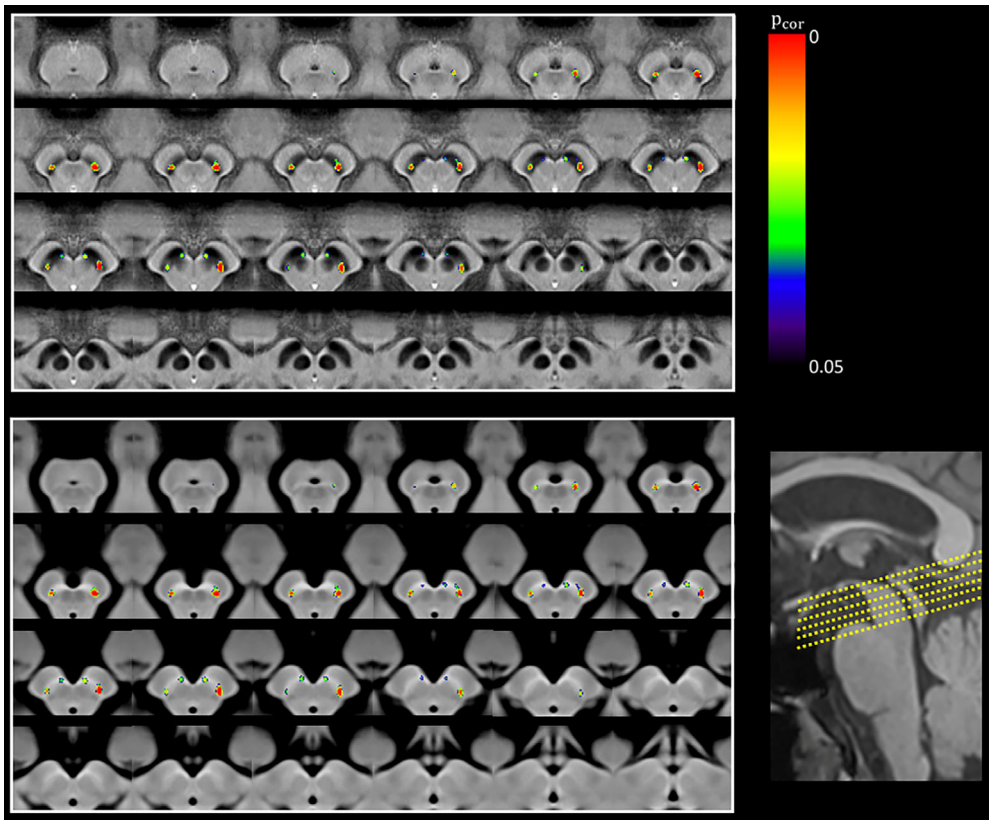

FIGURE 2 All images above are resampled perpendicular to the midbrain axis. A voxelwise analysis of neuromelanin-sensitive imaging between early-stage IPD patients and healthy subjects reveals two separate areas with significant statistical difference (a corrected *p* value <.05) in the substantia nigra (overlaid on SMwI [upper row] and NM-MRI templates [lower row]). All images are displayed using the radiological convention

TABLE 2 The ranges of contrast ratio (CR) values of the areas with significant group difference between IPD patients and healthy subjects on NM-MRI

	IPD patients (*n* = 50)				Healthy subjects (*n* = 50)			
	Minimum	**Maximum**	**Mean**	***SD***	**Minimum**	**Maximum**	**Mean**	***SD***
Significantly different regions	.089556	.217321	.141522	.031067	.097418	.264732	.175538	.031371
Whole SNpc	.076808	.189195	.127170	.025358	.108020	.274834	.183413	.0310916

Abbreviations: IPD, idiopathic Parkinson's disease; NM-MRI, neuromelanin-sensitive MRI; SNpc, the substantia nigra pars compacta.

with early-stage IPD. In accordance with previous results, this area is putatively the nigrosome 2 region (Massey et al., 2017; Schwarz et al., 2018). This observation may be supported by previous pathological results, in which nigrosome 1 is most significantly involved in IPD, followed by nigrosome 2, 4, 3, and 5 (Damier et al., 1999).

Our results are partly in line with those of a recent study, which suggested that, compared to healthy controls, the NM-MRI signal changes in the posterolateral aspect of the SNpc in early-stage IPD patients (Biondetti et al., 2020). However, unlike our results, in this study, they assessed volume differences on probability maps after manually segmenting the SNpc, and did not show the significantly affected region in the anteromedial aspect of the SNpc unlike our results. Different technical factors, including MR sequence and spatial resolution, as well as different analytic methods, may account for the discrepant results. Nevertheless, our imaging method has an advantage in terms of spatial resolution, and may be supported by the previous results indicating the nigrosome 2 region to be the second most significantly affected region.

A previous study claimed that, compared to healthy subjects, CR decreases are predominately noted in the ventrolateral (or anterolateral) aspects of SN in IPD patients (Cassidy et al., 2019). Although this study proved the correlation between NM-MRI signal and neuromelanin concentration, the voxelwise analysis results are different from ours and those from volume or CR measurements in previous studies. The ventrolateral tier is located in the posteroinferior aspect of the SNpc, and this region is known to be most significantly affected in IPD (Fearnley & Lees, 1991). Because the posteroinferior part of the SNpc is smaller than the anterosuperior subregion, it may be more easily affected by the partial volume effect. Additionally, a recent study suggested that 1.5 mm thick NM-MRI is recommended for voxelwise analysis because of its higher reliability (Wengler et al., 2020). Given the anatomical characteristics and a potential limitation in terms of slice resolution, the voxelwise analysis using 3 mm thick NM-MRI might lead to failure in determining abnormality in the posterior region of the SNpc and consequently determined predominate abnormality in the anterolateral region of the SN

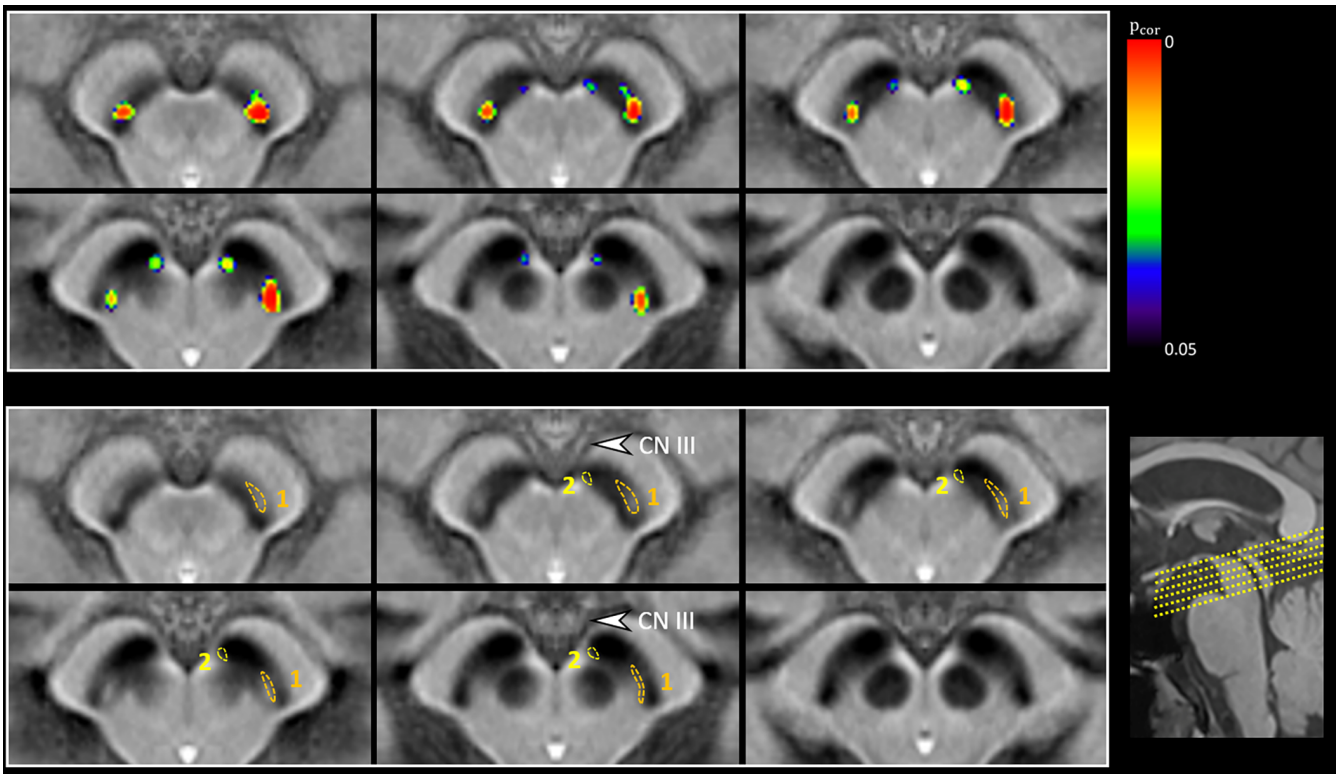

FIGURE 3 All images are resampled perpendicular to the midbrain axis. A voxelwise analysis of neuromelanin-sensitive imaging between early-stage IPD patients and healthy subjects reveals two separate areas with significant statistical difference (a corrected *p* value <.05) in the substantia nigra (overlaid on the SMwI [upper row]). The nigrosome 1 (orange dotted ovals) and nigrosome 2 (yellow dotted ovals) regions are overlaid on the SMwI template (lower row) in accordance with previous study (Massey et al., 2017). The oculomotor nerve (CN III) is indicated by arrowheads. All images are displayed using the radiological convention

TABLE 3 Cluster sizes and *p* values of the significantly different regions on NM-MRI between patients with idiopathic Parkinson's disease and healthy subjects

	Significantly different regions	Cluster size (mm^3)	*p* value*
NM-MRI	A region in the presumed left nigrosome 1	42.750	.0189
	A region in the presumed right nigrosome 1	14.375	.0273
	A region in the presumed left nigrosome 2	2.625	.0463
	A region in the presumed right nigrosome 2	1.125	.0476
SMwI	A region in the left substantia nigra	140.625	.0104
	A region in the right substantia nigra	77.625	.0184

*$p < .05$, TFCE-corrected.

(Cassidy et al., 2019). Patients in the cohorts with relatively longer disease durations (mean of 7.3 years, Cassidy et al., 2019; median 8 years [interquartile rage, 2–18], Oshima et al., 2020) may also explain the wider involvement in the anterolateral aspect of the SNpc.

Our study revealed that the abnormal region in the posterior aspect of the SNpc is larger on the left, which may be explained by the patients' characteristics. Of the 50 IPD patients in this study, 45 (90%) were right-handed. It has been reported that 59.5% of right-handed patients with IPD have right-dominant symptoms (van der Hoorn, Burger, Leenders, & de Jong, 2012), and it has also been shown that right-handed IPD patients revealed a lower specific binding ratio in the left putamen on dopamine transporter (DAT) single photon emission computed tomography (SPECT; Garrido et al., 2020). Given that the signal intensity in NM-MRI is correlated with neuromelanin content in the SN (Cassidy et al., 2019), and that DAT activity is reflected by the extent of dopaminergic neurons with neuromelanin in the SN (Kraemmer et al., 2014), it could be expected that our study cohort would reveal a greater affected region in the left SNpc. Nevertheless, it would be necessary to investigate further to find the cause of the size difference of the abnormal region between the right and left SNpc because 31 patients (62%) had right dominant symptoms.

In a recent study with an NM-MRI template ($0.8 \times 0.8 \times 2.5$ mm^3 with a 0.25 mm gap) in 30 patients with bilateral IPD (Martin-Bastida et al., 2019), the authors found that the CR of the ventral tier of the SNpc was lower than that of the dorsal tier. However, in regression

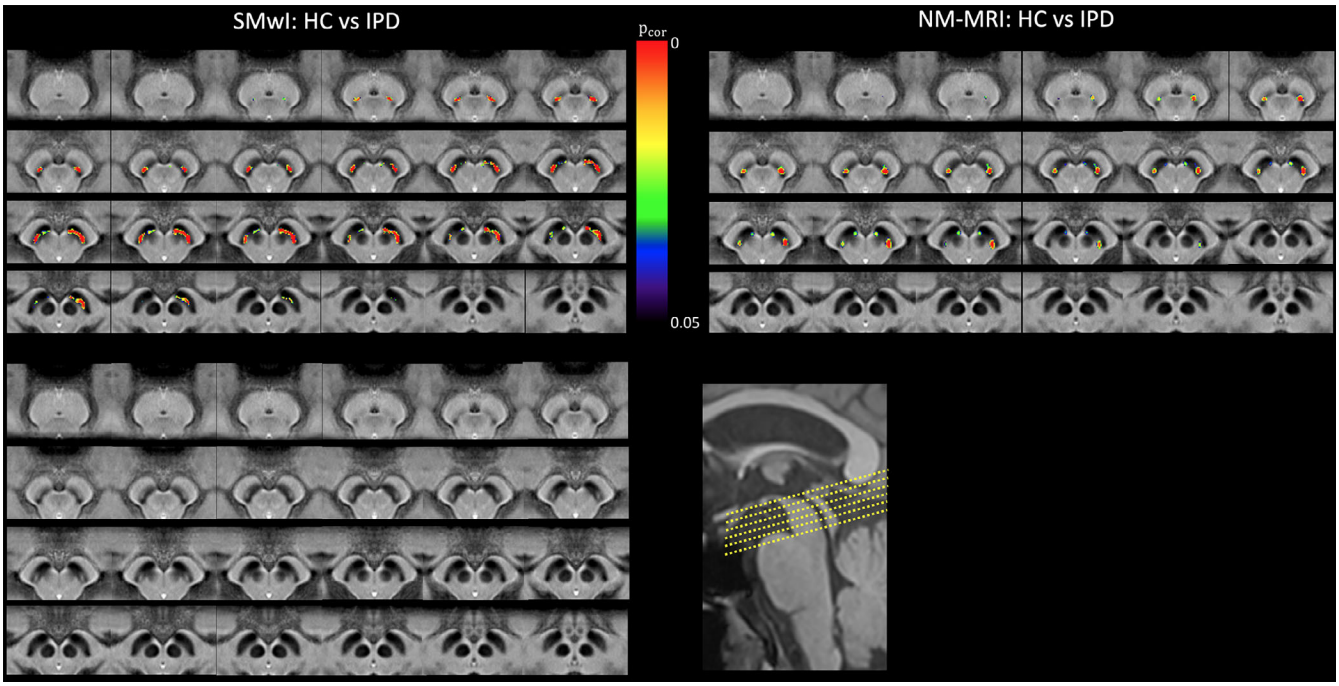

FIGURE 4 All images above are resampled parallel to the midbrain axis. A voxelwise analysis of SMwI between early-stage IPD patients and healthy subjects reveals two separate areas with significant statistical difference (a corrected *p* value <.05) in the substantia nigra (overlaid on the SMwI template [left in the upper row]). These areas of group difference on SMwI are slightly greater than those on NM-MRI (right in the upper row), including the areas showing group difference on NM-MRI. Also seen is that the area on the left is larger than that on the right, which is similarly noted on NM-MRI. The areas showing group difference on SMwI are slightly larger than the presumed nigrosome 1 and nigrosome 2 regions (Figure 3). All images are displayed using the radiological convention

analysis, there was no significant association between the CR of the SNpc and DAT activity. A significant relationship was only observed between the CR of the ventral tier of the SNpc and DAT activity for the side clinically defined as most affected. The authors arbitrarily defined the ventral and dorsal tiers using imaging with a relatively thicker slice (2.75 mm) but due to lack of a voxelwise analysis, they did not show which specific area in the SNpc was most significantly affected. They might have had better results if they had obtained thinner slice imaging and had drawn another region of interest in the posterior aspect of the SNpc, given the results by previous NM-MRI studies where they found that the posterolateral region of the SNpc was significantly affected in IPD (Ohtsuka et al., 2014; Prasad et al., 2018; Wang et al., 2018) and our results in which the most significantly affected region was located in the posterior aspect of the ventral tier on imaging parallel to the AC-PC line (Figure S5).

Despite using the CR values of the areas of group difference on NM-MRI, we failed to find significant correlations between the UPDRS III scores and the CR values of the areas of group difference. Significant correlation was also not found when using the CR values of the whole SNpc on NM-MRI. The latter result is in line with those of recent studies by using NM-MRI (Oshima et al., 2020; Vitali et al., 2020) in which they assessed the correlation between the UPDRS III scores and the CR values of the whole SNpc.

The areas showing group difference on SMwI are slightly larger than the presumed nigrosome 1 and nigrosome 2 regions in our study. A previous study in which the authors showed that the width of the SN on NM-MRI is not correlated with T2* values in early-stage IPD patients (Reimao et al., 2016). Their results may explain the size difference between NM-MRI and SMwI in terms of significant spatial difference in our study. Nonetheless, at this moment, we do not know why the areas of significant signal alteration exceed the presumed nigrosome 1 and nigrosome 2 regions on SMwI. Further study with pathological correlation may be warranted.

This present study had a few limitations. First, this was a single center study with specific imaging techniques, including SMwI based on multi-echo GRE imaging and NM-MRI based on 3D T1 SPACE with DANTE preparation. While the multi-echo GRE imaging for SMwI is similarly obtained across vendors, 3D T1 SPACE imaging, DANTE preparation, and the CAIPIRINHA technique for NM-MRI are proprietary or work-in-progress sequences. This may limit the general application of our NM-MRI in clinical practice or for research. Second, NM-MRI was used in our study to determine abnormality in the SNpc of IPD patients, but the results were not pathologically proven. Nevertheless, a recent study (Cassidy et al., 2019) showing the correlation between the NM-MRI signal and neuromelanin content in the SN may support our results. Also, in real practice, it is not easy to conduct autopsies on patients with early-stage IPD. Lastly, we did not assess the correlation between the uptake values on 18F-FP-CIT PET and the CR values of group difference on NM-MRI. However, we believe that this assessment is beyond the scope of the current study. For

such an analysis, it may be necessary to draw various regions of interest that include the ventral tier, two or three subdivisions, the presumed nigrosome 1 region based on SMwI, and the regions that we found in our NM-MRI study.

In summary, our voxelwise analysis with a thinner-slice template revealed that two regions in the SNpc are significantly different between early-stage IPD patients and healthy subjects. The larger region is located in the posterolateral aspect of the SNpc on both sides on NM-MRI, and in the posterior hyperintensity on the SMwI template, which may be in the nigrosome 1 region on SWI. The smaller region is noted in the anteromedial aspect of the SNpc on both sides, which may be in the nigrosome 2 region on SWI.

ACKNOWLEDGMENTS

This study was supported by a grant from the Korea Healthcare Technology R&D Project, through the Korea Health Industry Development Institute (KHIDI), funded by the Ministry of Health & Welfare, Republic of Korea (Grant No. HI14C1135); and a grant from the Brain Research Program of the National Research Foundation (NRF) funded by the Korean government (MSIT) (No. 2018M3C7A1056889).

ETHICS STATEMENT

This study was approved by the Institutional Review Board of the Gil Medical Center, Gachon University College of Medicine.

DATA AVAILABILITY STATEMENT

The data that support the findings of this study are available from the corresponding author upon reasonable request.

ORCID

Young Noh https://orcid.org/0000-0002-9633-3314
Eung Yeop Kim https://orcid.org/0000-0002-9579-4098

REFERENCES

Biondetti, E., Gaurav, R., Yahia-Cherif, L., Mangone, G., Pyatigorskaya, N., Valabregue, R., … Lehericy, S. (2020). Spatiotemporal changes in substantia nigra neuromelanin content in Parkinson's disease. *Brain*, *143*, 2757–2770. https://doi.org/10.1093/brain/awaa216

Cassidy, C. M., Zucca, F. A., Girgis, R. R., Baker, S. C., Weinstein, J. J., Sharp, M. E., … Horga, G. (2019). Neuromelanin-sensitive MRI as a noninvasive proxy measure of dopamine function in the human brain. *Proceedings of the National Academy of Sciences of the United States of America*, *116*(11), 5108–5117. https://doi.org/10.1073/pnas.1807983116

Castellanos, G., Fernandez-Seara, M. A., Lorenzo-Betancor, O., Ortega-Cubero, S., Puigvert, M., Uranga, J., … Pastor, M. A. (2015). Automated neuromelanin imaging as a diagnostic biomarker for Parkinson's disease. *Movement Disorders*, *30*(7), 945–952. https://doi.org/10.1002/mds.26201

Cho, J., Noh, Y., Kim, S. Y., Sohn, J., Noh, J., Kim, W., … Kim, C. (2020). Long-term ambient air pollution exposures and Brain imaging markers in Korean adults: The Environmental Pollution-Induced Neurological EFfects (EPINEF) study. *Environmental Health Perspectives*, *128*(11), 117006. https://doi.org/10.1289/EHP7133

Damier, P., Hirsch, E. C., Agid, Y., & Graybiel, A. M. (1999). The substantia nigra of the human brain. II. Patterns of loss of dopamine-containing neurons in Parkinson's disease. *Brain*, *122*(Pt 8), 1437–1448.

Fabbri, M., Reimao, S., Carvalho, M., Nunes, R. G., Abreu, D., Guedes, L. C., … Ferreira, J. J. (2017). Substantia Nigra Neuromelanin as an imaging biomarker of disease progression in Parkinson's disease. *Journal of Parkinson's Disease*, *7*(3), 491–501. https://doi.org/10.3233/JPD-171135

Fearnley, J. M., & Lees, A. J. (1991). Ageing and Parkinson's disease: Substantia nigra regional selectivity. *Brain*, *114*(Pt 5), 2283–2301.

Fonov, V., Evans, A. C., Botteron, K., Almli, C. R., McKinstry, R. C., Collins, D. L., & Brain Development Cooperative, G. (2011). Unbiased average age-appropriate atlases for pediatric studies. *NeuroImage*, *54*(1), 313–327. https://doi.org/10.1016/j.neuroimage.2010.07.033

Garrido, A., Iranzo, A., Stefani, A., Serradell, M., Munoz-Lopetegi, A., Marrero, P., … Sleep Innsbruck Barcelona, G. (2020). Lack of asymmetry of nigrostriatal dopaminergic function in healthy subjects. *Movement Disorders*, *35*(6), 1072–1076. https://doi.org/10.1002/mds.28019

Gho, S. M., Liu, C., Li, W., Jang, U., Kim, E. Y., Hwang, D., & Kim, D. H. (2014). Susceptibility map-weighted imaging (SMWI) for neuroimaging. *Magnetic Resonance in Medicine*, *72*(2), 337–346. https://doi.org/10.1002/mrm.24920

Hoehn, M. M., & Yahr, M. D. (1967). Parkinsonism: Onset, progression and mortality. *Neurology*, *17*(5), 427–442. https://doi.org/10.1212/wnl.17.5.427

Isaias, I. U., Trujillo, P., Summers, P., Marotta, G., Mainardi, L., Pezzoli, G., … Costa, A. (2016). Neuromelanin imaging and dopaminergic loss in Parkinson's disease. *Frontiers in Aging Neuroscience*, *8*, 196. https://doi.org/10.3389/fnagi.2016.00196

Kashihara, K., Shinya, T., & Higaki, F. (2011). Neuromelanin magnetic resonance imaging of nigral volume loss in patients with Parkinson's disease. *Journal of Clinical Neuroscience*, *18*(8), 1093–1096. https://doi.org/10.1016/j.jocn.2010.08.043

Kraemmer, J., Kovacs, G. G., Perju-Dumbrava, L., Pirker, S., Traub-Weidinger, T., & Pirker, W. (2014). Correlation of striatal dopamine transporter imaging with post mortem substantia nigra cell counts. *Movement Disorders*, *29*(14), 1767–1773. https://doi.org/10.1002/mds.25975

Kuya, K., Ogawa, T., Shinohara, Y., Ishibashi, M., Fujii, S., Mukuda, N., & Tanabe, Y. (2018). Evaluation of Parkinson's disease by neuromelanin-sensitive magnetic resonance imaging and (123)I-FP-CIT SPECT. *Acta Radiologica*, *59*(5), 593–598. https://doi.org/10.1177/0284185117722812

Langley, J., Huddleston, D. E., Chen, X., Sedlacik, J., Zachariah, N., & Hu, X. (2015). A multicontrast approach for comprehensive imaging of substantia nigra. *NeuroImage*, *112*, 7–13. https://doi.org/10.1016/j.neuroimage.2015.02.045

le Berre, A., Kamagata, K., Otsuka, Y., Andica, C., Hatano, T., Saccenti, L., … Aoki, S. (2019). Convolutional neural network-based segmentation can help in assessing the substantia nigra in neuromelanin MRI. *Neuroradiology*, *61*(12), 1387–1395. https://doi.org/10.1007/s00234-019-02279-w

Mahlknecht, P., Krismer, F., Poewe, W., & Seppi, K. (2017). Meta-analysis of dorsolateral nigral hyperintensity on magnetic resonance imaging as a marker for Parkinson's disease. *Movement Disorders*, *32*(4), 619–623. https://doi.org/10.1002/mds.26932

Martin-Bastida, A., Lao-Kaim, N. P., Roussakis, A. A., Searle, G. E., Xing, Y., Gunn, R. N., … Piccini, P. (2019). Relationship between neuromelanin and dopamine terminals within the Parkinson's nigrostriatal system. *Brain*, *142*(7), 2023–2036. https://doi.org/10.1093/brain/awz120

Massey, L. A., Miranda, M. A., Al-Helli, O., Parkes, H. G., Thornton, J. S., So, P. W., … Yousry, T. A. (2017). 9.4 T MR microscopy of the substantia nigra with pathological validation in controls and disease. *Neuroimage Clinical*, *13*, 154–163. https://doi.org/10.1016/j.nicl.2016.11.015

Matsusue, E., Fujihara, Y., Tanaka, K., Aozasa, Y., Shimoda, M., Nakayasu, H., … Ogawa, T. (2019). The utility of the combined use of

(123)I-FP-CIT SPECT and neuromelanin MRI in differentiating Parkinson's disease from other parkinsonian syndromes. *Acta Radiologica*, *60*(2), 230–238. https://doi.org/10.1177/0284185118778871

Nam, Y., Gho, S. M., Kim, D. H., Kim, E. Y., & Lee, J. (2017). Imaging of nigrosome 1 in substantia nigra at 3T using multiecho susceptibility map-weighted imaging (SMWI). *Journal of Magnetic Resonance Imaging*, *46*(2), 528–536. https://doi.org/10.1002/jmri.25553

Ogisu, K., Kudo, K., Sasaki, M., Sakushima, K., Yabe, I., Sasaki, H., … Shirato, H. (2013). 3D neuromelanin-sensitive magnetic resonance imaging with semi-automated volume measurement of the substantia nigra pars compacta for diagnosis of Parkinson's disease. *Neuroradiology*, *55*(6), 719–724. https://doi.org/10.1007/s00234-013-1171-8

Ohtsuka, C., Sasaki, M., Konno, K., Kato, K., Takahashi, J., Yamashita, F., & Terayama, Y. (2014). Differentiation of early-stage parkinsonisms using neuromelanin-sensitive magnetic resonance imaging. *Parkinsonism & Related Disorders*, *20*(7), 755–760. https://doi.org/10.1016/j.parkreldis.2014.04.005

Okuzumi, A., Hatano, T., Kamagata, K., Hori, M., Mori, A., Oji, Y., … Hattori, N. (2019). Neuromelanin or DaT-SPECT: Which is the better marker for discriminating advanced Parkinson's disease? *European Journal of Neurology*, *26*(11), 1408–1416. https://doi.org/10.1111/ene.14009

Oshima, S., Fushimi, Y., Okada, T., Nakajima, S., Yokota, Y., Shima, A., … Nakamoto, Y. (2020). Neuromelanin-sensitive magnetic resonance imaging using DANTE pulse. *Movement Disorders*. https://doi.org/10.1002/mds.28417

Postuma, R. B., Berg, D., Stern, M., Poewe, W., Olanow, C. W., Oertel, W., … Deuschl, G. (2015). MDS clinical diagnostic criteria for Parkinson's disease. *Movement Disorders*, *30*(12), 1591–1601. https://doi.org/10.1002/mds.26424

Prasad, S., Stezin, A., Lenka, A., George, L., Saini, J., Yadav, R., & Pal, P. K. (2018). Three-dimensional neuromelanin-sensitive magnetic resonance imaging of the substantia nigra in Parkinson's disease. *European Journal of Neurology*, *25*(4), 680–686. https://doi.org/10.1111/ene.13573

Pyatigorskaya, N., Magnin, B., Mongin, M., Yahia-Cherif, L., Valabregue, R., Arnaldi, D., … Lehericy, S. (2018). Comparative study of MRI biomarkers in the substantia nigra to discriminate idiopathic Parkinson's disease. *AJNR. American Journal of Neuroradiology*, *39*(8), 1460–1467. https://doi.org/10.3174/ajnr.A5702

Reimao, S., Ferreira, S., Nunes, R. G., Pita Lobo, P., Neutel, D., Abreu, D., … Ferreira, J. J. (2016). Magnetic resonance correlation of iron content with neuromelanin in the substantia nigra of early-stage Parkinson's disease. *European Journal of Neurology*, *23*(2), 368–374. https://doi.org/10.1111/ene.12838

Reimao, S., Pita Lobo, P., Neutel, D., Correia Guedes, L., Coelho, M., Rosa, M. M., … Ferreira, J. J. (2015). Substantia nigra neuromelanin magnetic resonance imaging in de novo Parkinson's disease patients. *European Journal of Neurology*, *22*(3), 540–546. https://doi.org/10.1111/ene.12613

Reimao, S., Pita Lobo, P., Neutel, D., Guedes, L. C., Coelho, M., Rosa, M. M., … Ferreira, J. J. (2015). Substantia nigra neuromelanin-MR imaging differentiates essential tremor from Parkinson's disease. *Movement Disorders*, *30*(7), 953–959. https://doi.org/10.1002/mds.26182

Schwarz, S. T., Mougin, O., Xing, Y., Blazejewska, A., Bajaj, N., Auer, D. P., & Gowland, P. (2018). Parkinson's disease related signal change in the nigrosomes 1-5 and the substantia nigra using T2* weighted 7T MRI. *Neuroimage Clinical*, *19*, 683–689. https://doi.org/10.1016/j.nicl.2018.05.027

Schwarz, S. T., Rittman, T., Gontu, V., Morgan, P. S., Bajaj, N., & Auer, D. P. (2011). T1-weighted MRI shows stage-dependent substantia nigra signal loss in Parkinson's disease. *Movement Disorders*, *26*(9), 1633–1638. https://doi.org/10.1002/mds.23722

Schwarz, S. T., Xing, Y., Tomar, P., Bajaj, N., & Auer, D. P. (2017). In vivo assessment of brainstem depigmentation in Parkinson disease: Potential as a severity marker for multicenter studies. *Radiology*, *283*(3), 789–798. https://doi.org/10.1148/radiol.2016160662

Sled, J. G., Zijdenbos, A. P., & Evans, A. C. (1998). A nonparametric method for automatic correction of intensity nonuniformity in MRI data. *IEEE Transactions on Medical Imaging*, *17*(1), 87–97. https://doi.org/10.1109/42.668698

Smith, S. M. (2002). Fast robust automated brain extraction. *Human Brain Mapping*, *17*(3), 143–155. https://doi.org/10.1002/hbm.10062

Sung, Y. H., Lee, J., Nam, Y., Shin, H. G., Noh, Y., Shin, D. H., & Kim, E. Y. (2018). Differential involvement of nigral subregions in idiopathic Parkinson's disease. *Human Brain Mapping*, *39*(1), 542–553. https://doi.org/10.1002/hbm.23863

Takahashi, H., Watanabe, Y., Tanaka, H., Mihara, M., Mochizuki, H., Takahashi, K., … Tomiyama, N. (2018). Comprehensive MRI quantification of the substantia nigra pars compacta in Parkinson's disease. *European Journal of Radiology*, *109*, 48–56. https://doi.org/10.1016/j.ejrad.2018.06.024

Taniguchi, D., Hatano, T., Kamagata, K., Okuzumi, A., Oji, Y., Mori, A., … Hattori, N. (2018). Neuromelanin imaging and midbrain volumetry in progressive supranuclear palsy and Parkinson's disease. *Movement Disorders*, *33*(9), 1488–1492. https://doi.org/10.1002/mds.27365

van der Hoorn, A., Burger, H., Leenders, K. L., & de Jong, B. M. (2012). Handedness correlates with the dominant Parkinson side: A systematic review and meta-analysis. *Movement Disorders*, *27*(2), 206–210. https://doi.org/10.1002/mds.24007

Vitali, P., Pan, M. I., Palesi, F., Germani, G., Faggioli, A., Anzalone, N., … Gandini Wheeler-Kingshott, C. A. M. (2020). Substantia Nigra Volumetry with 3-T MRI in de novo and advanced Parkinson disease. *Radiology*, *296*(2), 401–410. https://doi.org/10.1148/radiol.2020191235

Wang, J., Li, Y., Huang, Z., Wan, W., Zhang, Y., Wang, C., … Jin, L. (2018). Neuromelanin-sensitive magnetic resonance imaging features of the substantia nigra and locus coeruleus in de novo Parkinson's disease and its phenotypes. *European Journal of Neurology*, *25*(7), 949–e973. https://doi.org/10.1111/ene.13628

Wengler, K., He, X., Abi-Dargham, A., & Horga, G. (2020). Reproducibility assessment of neuromelanin-sensitive magnetic resonance imaging protocols for region-of-interest and voxelwise analyses. *NeuroImage*, *208*, 116457. https://doi.org/10.1016/j.neuroimage.2019.116457

Xiang, Y., Gong, T., Wu, J., Li, J., Chen, Y., Wang, Y., … Du, Y. (2017). Subtypes evaluation of motor dysfunction in Parkinson's disease using neuromelanin-sensitive magnetic resonance imaging. *Neuroscience Letters*, *638*, 145–150. https://doi.org/10.1016/j.neulet.2016.12.036

Zupan, G., Suput, D., Pirtosek, Z., & Vovk, A. (2019). Semi-automatic signature-based segmentation method for quantification of Neuromelanin in Substantia Nigra. *Brain Sciences*, *9*(12), 335. https://doi.org/10.3390/brainsci9120335

SUPPORTING INFORMATION

Additional supporting information may be found online in the Supporting Information section at the end of this article.

How to cite this article: Sung YH, Noh Y, Kim EY. Early-stage Parkinson's disease: Abnormal nigrosome 1 and 2 revealed by a voxelwise analysis of neuromelanin-sensitive MRI. *Hum Brain Mapp*. 2021;42:2823–2832. https://doi.org/10.1002/hbm.25406